

Spontaneous emergence of space stems ahead of negative leaders in lightning and long sparks

A. Malagón-Romero¹, A. Luque¹

¹IAA-CSIC, P.O. Box 3004, 18080, Granada, Spain

Key Points:

- Space stems start as regions of locally lower conductivity in the streamer channels around the tip of negative leaders.
- An attachment instability enhances the electric field at the space stem decreasing further the conductivity and leading to bright and locally warmer regions.
- As the attachment instability is favoured by high electric fields inside negative streamer channels it explains why only negative leaders propagate in long steps.

Abstract

We investigate the emergence of space stems ahead of negative leaders. These are luminous spots that appear ahead of an advancing leader mediating the leader's stepped propagation. We show that space stems start as regions of locally depleted conductivity that form in the streamers of the corona around the leader. An attachment instability enhances the electric field leading to strongly inhomogeneous, bright and locally warmer regions ahead of the leader that explain the existing observations. Since the attachment instability is only triggered by fields above 10 kV/cm and internal electric fields are lower in positive than in negative streamers, our results explain why, although common in negative leaders, space stems and stepping are hardly observed if not absent in positive leaders. Further work is required to fully explain the streamer to leader transition, which requires an electric current persisting for timescales longer than the typical attachment time of electrons, around 100 ns.

Plain Language Summary

Long electrical discharges of negative polarity, such as most cloud-to-ground lightning flashes, propagate in a stepped manner, i.e. alternating between standing and jumping suddenly. The underlying mechanism explaining this behavior is not well understood, although we know that space stems are a key element. These are bright and locally warmer segments that appear ahead of a discharge channel and apparently isolated from it. For the first time, we show how these space stems emerge spontaneously in our simulations from regions of locally lower conductivity that latter become bright and warm. Then on one hand we propose a possible origin of the space stems and, on the other hand, we shed some light on possible mechanisms that grow these stems to longer times, beyond 100 ns.

1 Introduction

One of the outstanding mysteries in atmospheric electricity concerns the progression of negative lightning leaders. Being hot and ionized channels, leaders are initiated in a thundercloud and expand bipolarly, with their positive and negative extremes advancing in more or less opposite directions. For some elusive reason, negative leaders advance in a stepped fashion, with waiting times of tens of microseconds punctuated by sudden jumps of microsecond timescale (Dwyer & Uman, 2014). This behavior is observed not only in lightning leaders but also in negative laboratory discharges longer than about two meters.

Besides being a fundamental but mysterious process in electrical discharges, leader steps are relevant because they produce the Very High Frequency (VHF) radio pulses that reveal the development of lightning flashes in Lightning Mapping Arrays (Thomas et al., 2001).

Leader steps are also correlated with X-ray emissions detected around a lightning discharge (Dwyer et al., 2005) and therefore they are possibly linked to Terrestrial Gamma-ray Flashes (TGFs) detected by satellites orbiting hundreds of kilometers above ground (Briggs et al., 2013; Fishman et al., 1994; Marisaldi et al., 2010; Smith, Lopez, Lin, & Barrington-Leigh, 2005).

The first observation of leader stepping can be traced back to the pioneering work of Schonland, Malan, and Collens (1935) in the 1930s, who coined the term “stepped leader” for the intermittent advance of downward negative lightning channels recorded in their streak camera. In the decades after Schonland’s work, advances in this topic arose mostly from laboratory experiments with meter-long spark discharges. The work of, among others, Gorin, Levitov, and Shkilev (1976) and the Les Renardières group (1978) revealed the dynamics of a negative leader step: the leader tip is preceded by a filamentary corona containing a bright nucleus termed “space stem”. After some microseconds the space stem evolves into a “space leader” that propagates in both directions and whose extremes are surrounded by additional coronas of both polarities. The leader completes one step when the space leader bridges the gap to the main leader channel.

Recordings with the high-framerate video cameras fielded in the last decade show that lightning leaders, although they involve slightly different space- and time-scales, follow the same pattern as long laboratory sparks. With integration times of a few microseconds, the observations of Hill, Uman, and Jordan (2011) for natural stepped leaders and Biagi, Uman, Hill, and Jordan (2014) and Gamerota et al. (2014) for leaders in triggered lightning captured images of the space stem ahead of the leader tip, embedded in a filamentary corona.

Despite these observational advances, our understanding about the physics of stepped leaders is still very incomplete. Measured optical spectra indicate that the leader temperature reaches around 5000 K (Cooray, 2003) for laboratory discharges and up to 30 000 K in lightning leaders (Orville, 1968), which, in both cases and according to chemical models, suffices to sustain a high ionization (Gallimberti, 1979). On the other hand the filaments in the corona, called streamers, are not much above ambient temperature; their ionization, lower than that of leaders, is created mostly at their tips, where they enhance the electric field strongly enough to accelerate electrons up to the threshold of impact ionization (Ebert et al., 2010). Models for the streamer-to-leader transition (da Silva & Pasko, 2013; Popov, 2003) successfully reproduce the transition timescale of around 1 μ s for atmospheric pressure but depend on manually imposing a total electric current that in reality is an outcome of the discharge physics. They also neglect the longitudinal inhomogeneity of the discharge and therefore they sideline leader stepping and the formation of space stems. The physical mechanism governing the latter re-

mains a mystery (see e.g. (Bazelyan & Raizer, 2010; Biagi et al., 2010)); a recent review (Dwyer & Uman, 2014) included this problem in the top ten questions in lightning research.

In this letter we show that space stems originate from an attachment instability inside streamer channels. Since space stems are the key to leader stepping, our results open the door to the full understanding of this mechanism as well as its associated radio and energetic particle emissions. Originally investigated in the 1970s (Douglas-Hamilton & Mani, 1974; Sigmond, 1984), the attachment instability is triggered by regions of lower conductance per unit length (i.e. conductivity integrated over a cross-section) inside a corona, which we show arise spontaneously when a negative streamer emerges from a leader. One major and slightly counter-intuitive aspect of our work is that bright regions inside a corona reveal regions of lower, not higher, electron density. Although this is in complete correspondence with a regular electrical circuit where energy is mostly dissipated in high-resistivity components, this insight has escaped previous interpretations of the space stem. At high-altitude, in leader-less discharges (sprites), the attachment instability forms standing patterns called beads and glows (Liu, 2010; Luque & Ebert, 2010; Luque, Stenbaek-Nielsen, McHarg, & Haaland, 2016).

2 Model

Since lightning leaders and long laboratory sparks share the same mechanism of propagation, to simplify our computations we choose to focus here on the propagation of a leader under laboratory conditions. Typical laboratory leaders span from tens of centimeters to around one meter and are surrounded by streamer coronas with roughly the same extension (Kostinskiy et al., 2018). These dimensions are too computationally demanding so, as we detail below, our simulated system is somewhat smaller.

Even then and despite recent progress in three-dimensional streamer simulations (Luque & Ebert, 2014; Shi, Liu, & Dwyer, 2017; Teunissen & Ebert, 2017), a full corona around a leader is presently out of reach for numerical models. We opt for simulating a single streamer that emerges from a leader tip; our assumption here is that the surrounding corona is not an essential component of the physics of space stems. We cannot rigorously justify this assumption but it is beared out by the similarity between observations and our results.

We thus investigate the formation of space stems ahead of a negative leader channel with a 2D cylindrically symmetric model (z, r) for electric discharges that includes heating and expansion of the background gas fully self-consistently. The background gas follows the equation of state for an ideal gas and its dynamics is described by the compressible Euler equations (da Silva & Pasko, 2013; Landau & Lifshitz, 1987; Popov, 2003). These are conservation equations for mass, momentum and energy:

$$\frac{\partial \rho}{\partial t} + \mathbf{u} \cdot \nabla \rho + \rho \nabla \cdot \mathbf{u} = 0, \quad (1a)$$

$$\frac{\partial \mathbf{u}}{\partial t} + (\mathbf{u} \cdot \nabla) \mathbf{u} + \frac{\nabla p}{\rho} = 0, \quad (1b)$$

$$\frac{\partial \varepsilon}{\partial t} + \mathbf{u} \cdot \nabla \varepsilon + \frac{p}{\rho} \nabla \cdot \mathbf{u} = \frac{w}{\rho}. \quad (1c)$$

Here ρ is the mass density of air, \mathbf{u} is the local velocity at a given point and time, p is the pressure and ε is the specific energy associated to the rotational and translational degrees of freedom, which we assume in thermal equilibrium. Finally, w is the local dissipated energy from the electric discharge. By using equations (1) and the equation of state for an ideal gas, we neglect thermal conduction and viscous dissipation, which have little effect on the time-scale of around 100 ns on which space stems form.

All species are advected along with the fluid with a velocity \mathbf{u} . Furthermore, charged species drift on top of the background gas motion according to the local value of the electric field \mathbf{E} , so the resulting velocity is $\mathbf{v}_s = \mathbf{u} + \mu_s \mathbf{E}$, where s labels the species and μ_s is the corresponding mobility. In our model, the dynamics of all charged species is described by diffusion-drift-reaction equations for electrons and ions,

$$\frac{\partial n_s}{\partial t} + \nabla \cdot (n_s \mathbf{v}_s) = C_s + \nabla \cdot (D_s \nabla n_s), \quad (2)$$

where n_s is the number density, D_s is the diffusion coefficient and C_s is the net production of species s .

The kinetic scheme employed in our simulations includes impact ionization, attachment/detachment, and water cluster formation and breaking. A detailed description of the scheme can be found in the supplementary material of Luque, González, and Gordillo-Vázquez (2017). The only difference is that for the three-body attachment reaction



here we have used the rate from Kossyi, Kostinsky, Matveyev, and Silakov (1992).

We emphasize the presence of water in the chemical model of our simulations. The relevance of water vapor for the evolution of streamer channels was previously discussed by Gallimberti (1979) and Luque et al. (2017). By clustering around negative ions, even a small quantity of water molecules effectively suppresses electron detachment and thus strongly influences the evolution of the electron density on timescales of tens of nanoseconds.

The electric field $\mathbf{E} = -\nabla \phi$ is determined by the balance of charged species and satisfies

$$-\nabla \cdot \mathbf{E} = \nabla^2 \phi = - \sum_s \frac{q_s n_s}{\epsilon_0}, \quad (4)$$

where q_s is the charge of species s and ϵ_0 is the vacuum permittivity, which we assume is also valid for air.

Streamer discharges develop as thin and elongated channels which call for a narrow computational domain. To achieve this while suppressing the influence of the radial boundary conditions in the Poisson's equation we use the domain decomposition method described by Malagón-Romero and Luque (2018). With this method we first find the electrostatic potential created by the space charges with a homogeneous Dirichlet boundary at $z = 0$ and free conditions in all other boundaries, meaning that the potential decays to zero at large distances. To the potential obtained in this manner we add a potential $\phi_0 = -E_0 z$ that accounts for an external electric field E_0 . The full domain size is $25 \text{ cm} \times 3 \text{ cm}$.

The term w couples the electrodynamics and bulk gas dynamics and accounts for dissipated power due to the electric current inside the corona. But note that this power is distributed unequally among the degrees of freedom of the underlying gas. Since the time-scales involved in the streamer-to-leader transition are too short to reach thermodynamic equilibrium, the fraction of energy deposited into different degrees of freedom depends on the local conditions and, in particular, on the local electric field (da Silva & Pasko, 2013; Flitti & Pancheshnyi, 2009). A small fraction is directly converted into translational energy of gas molecules and quickly thermalized. A larger amount excites electronic and ionization states; this is responsible for the process of *fast-heating* (Popov, 2001) and relaxes into thermal energy at timescales on the order of 100 ns. Another fraction of the energy is spent in dissociation of oxygen and nitrogen molecules and, finally, the remaining energy excites vibrational states and its time to thermalization is on the order of one second at ambient temperature and only significant compared with our relevant timescales once the temperature reaches about 10^4 K : this relaxation is neglected in the present study. Since, as we describe later, most heating is due to energies dissipated at or around the conventional breakdown electric field, roughly 30 kV/cm , we take the energy branching ratios corresponding to this field, where about half of the energy is frozen into vibrational excitations (see e.g. figure 1 in (Flitti & Pancheshnyi, 2009)). Furthermore, since the characteristic time of gas temperature increase is much longer than 100 ns, for the sake of simplicity, we consider fast-heating to be instantaneous. Then, we arrive at

$$w = \eta \mathbf{j} \cdot \mathbf{E}, \quad (5)$$

where $\eta \approx 0.5$ and $\mathbf{j} = \sum_s q_s n_s \mathbf{v}_s$.

Our initial condition consists in a short portion of leader with an small ionization patch slightly ahead of the tip that mimicks an irregularity of the leader head. The initial electron density is thus the sum of an uniform background n_e^{bg} plus

$$n_e^{\text{leader}} = n_{e0} \exp \left(-\frac{\max(z - z_L, 0)^2}{2\sigma_L^2} - \frac{r^2}{2\sigma_L^2} \right), \quad (6a)$$

and

$$n_e^{\text{seed}} = n_{e0} \exp\left(-\frac{(z - z_S)^2}{2\sigma_S^2} - \frac{r^2}{2\sigma_S^2}\right), \quad (6b)$$

where the tip location is $z_L = 5$ cm, the seed center is at $z_S = 6.1$ cm, the e -folding lengths are $\sigma_L = 3$ mm, $\sigma_S = 1.5$ mm and the electron density peaks at $n_{e0} = 10^{21} \text{ m}^{-3}$. The initial electron density is neutralized by an identical density of positive ions. Note that we selected these initial conditions after a few trials where we disregarded cases in which the streamer branches because these cannot be captured by our cylindrically symmetrical model. Besides, as mentioned above, to keep our computations feasible, the initial leader is somewhat shorter than experimental stepped leaders.

We have run two different simulations: one with photo-ionization ($n_e^{\text{bg}} = 0$) following the method presented by Luque, Ebert, Montijn, and Hundsdoerfer (2007), and another with a pre-conditioning of the gas surrounding the leader due to preceding coronas by adding a constant background ionization level $n_e^{\text{bg}} = 10^{15} \text{ m}^{-3}$. In both cases, we observed similar formation of a space stem but the simulation with photo-ionization exhibited an oscillation of the electric field at the streamer head that we attribute to a numerical artifact due to insufficient resolution for the smallest length scales involved in photo-ionization (Wormeester, Pancheshnyi, Luque, Nijdam, & Ebert, 2010; Zhelezniak, Mnatsakanian, & Sizykh, 1982). Henceforth we limit ourselves to the simulation without photo-ionization. To check that this does not affect our key results we used another numerical code at our disposal (PESTO, described by Luque (2017)) that includes photoionization but does not account for gas heating or long-term chemistry. Using PESTO, we run simulations with a numerical resolution of $6 \mu\text{m}$ that produced results similar to those described below.

The embedding gas is a mixture of 79% N_2 and 21% O_2 . Initially, the gas pressure is 1 atm and the mechanical energy is zero. The ambient temperature is 300K and the temperature of the leader follows the same distribution as n_e^{leader} with a peak value of 2700K. Note that our model does not include high-temperature chemistry for the leader: in our simulation the role of leader is merely to provide the electrostatic environment for the streamer propagation. Finally, the simulation is driven by an external electric field pointing towards the leader with magnitude $|E_0| = 10 \text{ kV/cm} + (20 \text{ kVcm}^{-1} \mu\text{s}^{-1})t$, where t is the simulation time.

With these conditions we simulated the inception and propagation of a streamer emerging from the leader tip. Our total simulation time was limited to about 100 ns at which point the streamer leaves the simulation domain. As we see below, this time is enough to see the formation of the space stem but too short to observe the full streamer-to-leader transition.

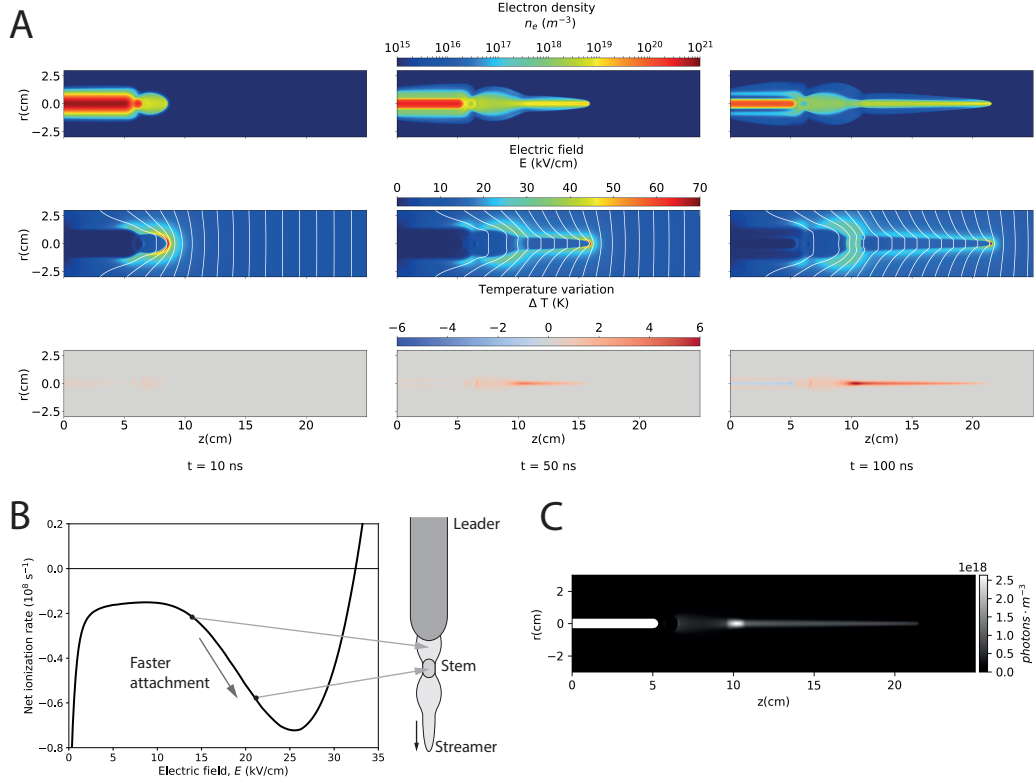


Figure 1. As a streamer propagates out of a leader tip it creates a segment of reduced conductivity that evolves into a space stem. Panel A summarizes the evolution of the streamer in terms of the electron density (top), electric field (middle), and temperature (bottom). The electric field row includes equipotential lines with constant spacing 12.5 kV, 13.5 kV and 14.5 kV (from left to right). The streamer leaves in its wake a segment of lower conductance per unit length that evolves into a space stem due to the attachment instability process sketched in panel B: a higher electric field accelerates the depletion of electrons, which in turns enhances the electric field. Finally, in panel C we show that our simulation reproduces the features of a space stem by plotting light emitted in the second positive system of the nitrogen molecule during the full simulation. We have masked (white region) leader emissions to focus on the space stem.

3 Results

Figure 1A summarizes our simulation. As the streamer emerges from the leader it goes through a narrowing phase where the conductance per unit length decreases. The charge transport through the streamer channel tends to homogenize the electric current flowing across the streamer channel, which implies a higher electric field in the narrow section. As sketched in figure 1B, where we plot the effective ionization rate of air, this enhanced field triggers an attachment instability (Luque et al., 2016): the higher field increases the rate of associative electron attachment, decreasing further the conductance per unit length and increasing the field. This process enhances the electric field inside the narrow section of the channel until it saturates at an electric field where the net ionization curve slopes upward, between 25 and 30 kV/cm. A necessary condition for this process is that the electric field inside the streamer channel steps above the minimum of the effective attachment rate, around 10 kV/cm (see figure 1B). The emergence of space stems is thus favoured in streamers with high internal electric fields.

To check that the narrow segment with an enhanced electric field reproduces the observed features of a space stem, we computed the spatial distribution of light emissions. We included in our model the electron impact excitation of nitrogen molecules to the $N_2(B^3\Pi_g)$ and $N_2(C^3\Pi_u)$ electronic states, which are responsible respectively of the first and second positive systems of N_2 (see the Supporting Information (Alghamdi et al., 2011; Balay et al., 2016a, 2016b; Capitelli, M., F., & I., 2000; Clawpack Development Team, 2017; Hagelaar & Pitchford, 2005; LeVeque, 2002; Nijdam, Takahashi, Markosyan, & Ebert, 2014) for further details on the chemistry used to describe light emissions). We found that in our conditions the emissions of light are dominated by the second positive system and panel C of figure 1 shows these emissions integrated over the 100 ns of simulation. There we notice a bright spot embedded in a dim channel, clearly reminiscent of images in high-speed recordings of leader progression (Biagi et al., 2014; Gamera et al., 2014; Hill et al., 2011). Based on this resemblance we will henceforth use the name *stem* for this bright nucleus within the channel.

Let us now analyze the gas heating produced by the discharge. This is represented in the bottom row of panel A in figure 1, where we show the temperature variation relative to the initial conditions. The air in the stem heats up about 6 K in 100 ns. However, in our simulation the electron density decreases both in the stem and in the surrounding channel with a time scale close to 100 ns. This is consistent with previous models and experiments that investigated the effect of the repetition rate in streamer discharges (Nijdam et al., 2014) and therefore it is unlikely that this electron depletion is due to shortcomings of our model. In our context it implies that the heating ratio diminishes: we do not expect a much higher temperature even if, by increasing our domain size, we extended our simulation time.

3.1 Formation of the Space Stem

Our key result is that the attachment instability is responsible for locally warmer regions ahead of a leader. A number of processes may reduce the channel conductance per unit length and trigger the instability, among them a jittering of the leader potential during the streamer propagation or pre-existing conductivity or gas-density perturbations along the streamer path (Luque & Gordillo-Vázquez, 2011; Luque et al., 2016). Neither of these processes was included in our simulations and nevertheless the space stem formed spontaneously, which suggests that isolated stems are robust features of leader propagation.

In our simulation the stem results from a narrowing of the channel. Note that the narrowing of negative streamers ahead of a leader or a pointed electrode has been observed by P. O. Kochkin, van Deursen, and Ebert (2014) and by Kostinskiy et al. (2018). As we show in figure 2 the streamer head is initially wide because it is affected by the divergence of electric field lines emerging from the leader's curved tip. As this divergence decreases away from the leader tip, the streamer head shrinks. The narrowing of the streamer channel enhances more strongly the electric field at the tip, increasing the degree of ionization left in the streamer head's wake. The total conductance per unit length of the channel scales approximately as $R^2 n_e$, where R is the channel radius and n_e the electron density: initially the significant decrease of the radius dominates and the conductance per unit length diminishes; afterwards the increase of n_e due to a higher field at the tip overcomes the narrowing and the conductance per unit length increases again. The resulting minimum is the origin of the space stem as we show in the upper panel of 3. In the same figure (lower panel) and as we stated before, despite the noticeable variation of the conductance per unit length, the intensity is homogeneous across any section of the channel, including the space stem.

Let us now discuss the observed asymmetry between positive and negative leaders. Stepping is more prominent and readily observable in negative leaders but there are now clear observations (Kostinskiy et al., 2018) that under conditions of high relative humidity, positive leaders also experience stepped progression although space stems have never been observed in positive leaders. Our results provide a natural explanation for this asymmetry: the attachment instability is triggered by elevated electric fields inside a streamer channel and due to stronger ionization in positive streamers, these fields are higher in negative streamers (Luque, Ratushnaya, & Ebert, 2008) for the same external field. Besides, positive streamers are initiated more easily (Liu, Kosar, Sadighi, Dwyer, & Rassoul, 2012) so they are launched from the leader tip at a lower potential and thus a lower driving electric field than negative streamers. To check this explanation we run simulations of positive streamers under driving electric fields of 10 kV/cm and 7 kV/cm; there the attachment instability was triggered only in regions of

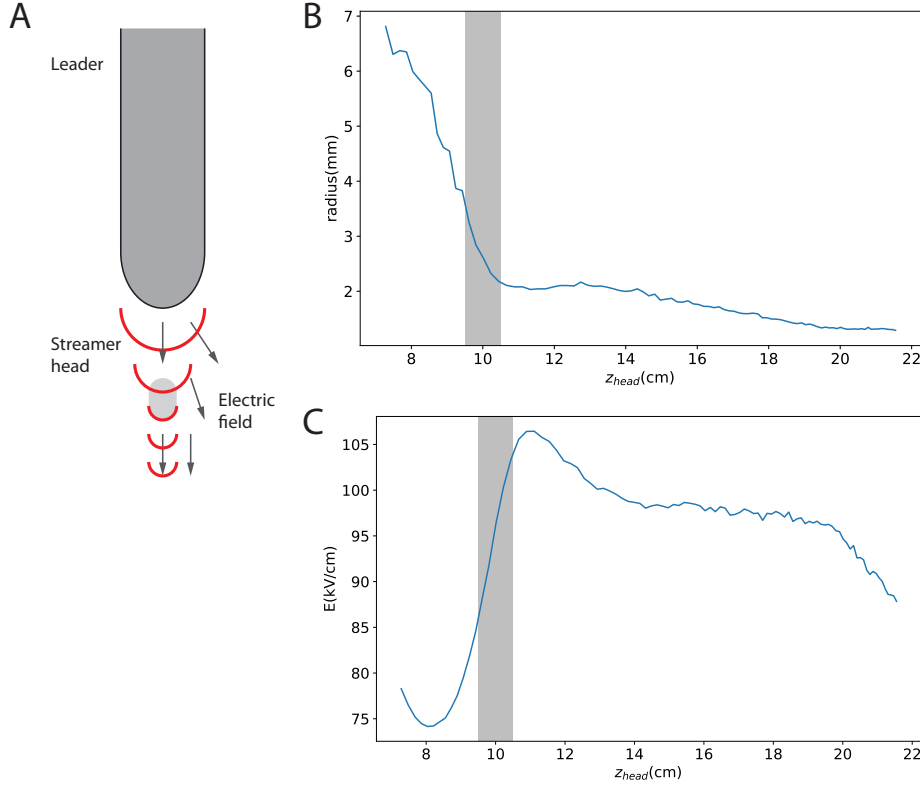


Figure 2. The space stem emerges due to the narrowing of the streamer channel. As sketched in panel A, when the streamer is still close to the leader tip it is widened by the diverging electric field lines around the curved leader tip; as it distances itself from the leader, the streamer is driven by a more homogeneous electric field and becomes narrower. This is shown in panel B, where we plot the streamer radius as a function of time. The radius is defined here as the radius of curvature on the central axis of the surface defined by the maximum of the electric in the z direction around the head. The reduction of the radius leads to higher peak electric fields (panel C) and the resulting total channel conductance per unit length exhibits a minimum that afterwards evolves into the space stem as described in figure 1.

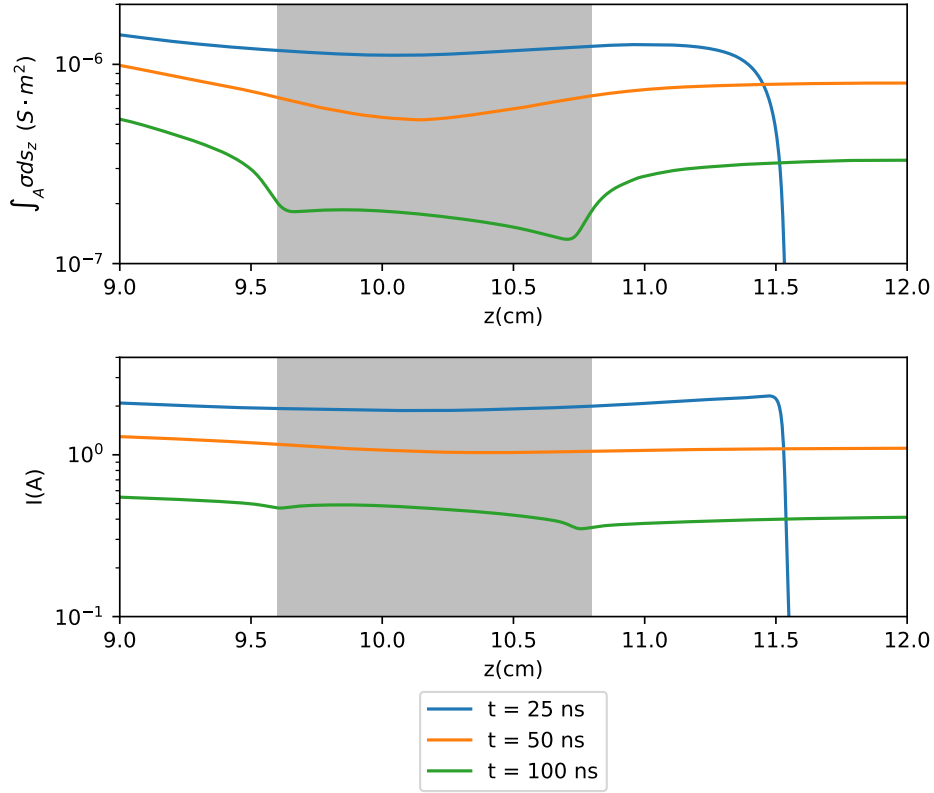


Figure 3. The upper panel shows the conductance per unit length around the space stem (grey area) at 25 ns, 50 ns and 100 ns. As the streamer propagates away from the leader tip (25 ns curve), the channel undergoes a narrowing until the conductance per unit length reaches a minimum (space stem). Right after, the channel starts to be able to compensate this narrowing with an increase of the electron density produced by a higher electric field and then the conductance per unit length rises. The two remaining curves show latter states of the conductance at the space stem, where the electron depletion is clear after attachment instability effects. The lower panel supports the idea that the low conductance in the space stem is countered by a high electric field to achieve an homogeneous intensity along the channel.

the channel very close to the leader tip, supporting the idea that steps in positive leaders exist but they are so small that isolated space stems cannot be observed.

4 Discussion and Conclusions

Our simulations show that the attachment instability explains the features of space stems ahead of propagating leaders. However at around 100 ns the overall conductivity of a streamer channel decays, stalling the increase in temperature. Our results thus stress the role in maintaining the corona played by poorly understood processes such as the inception of counter-propagating streamers (P. Kochkin, Lehtinen, van Deursen, & Østgaard, 2016; Luque et al., 2016) or the propagation of successive ionization waves along pre-existing channels (L. P. Babich, Bochkov, Kutsyk, Neubert, & Chanrion, 2015; Nijdam et al., 2014; Phelps, 1974; Rison et al., 2016). Previous models (da Silva & Pasko, 2013; Popov, 2003) missed the relevance of these processes because they were not self-consistent and set a constant current intensity in the channel. In these models a reduction of the electron density is immediately counteracted by an increase in the applied electric field so electrons are never significantly depleted. However, no physical mechanism with such an effect has been described in the literature.

As we have already shown, a single streamer discharge is unable to dissipate enough power to transit into a leader. Nonetheless, the relatively poor conductivity of a streamer corona together with a variable potential at the leader tip imply that there is often a significant electric field within the corona. This field triggers either new streamer bursts, as observed by P. O. Kochkin et al. (2014) or ionization waves retracing previous streamers, as proposed by L. P. Babich et al. (2015). It is also responsible for counter-streamers seeded by charges in existing stems. Remarkably, all of these mechanisms have been linked to X-ray emissions from long sparks (L. Babich & Bochkov, 2017; L. P. Babich et al., 2015; Ihaddadene & Celestin, 2015; P. O. Kochkin, van Deursen, & Ebert, 2015; Köhn, Chanrion, & Neubert, 2017; Luque, 2017; Østgaard et al., 2016) and these X-rays are in turn linked to leader stepping (Dwyer et al., 2005).

To check that these mechanisms may indeed explain the streamer-to-leader transition within the currently established observational constraints, we have developed a simplified model of a leader corona that we describe in the Supporting Information. The model shows that ionization waves increasing the electron density a factor of ten and repeating every 100 ns would lead to a significant increase of the temperature of the channel. But the main outcome is that a small difference in initial electron density in the stem leads to large differences in the heating rate of this segment compared to the rest of the corona.

An important simplification of our model is the assumption that a space stem can form within a single streamer channel and that streamer branching, even if present, is not an essential ingredient in the process. We base this assumption in two key observations: (1) space stems are generally observed as bright segments within longer, dimmer channels (Biagi et al., 2010; Hill et al., 2011) and (2) in laboratory images negative streamer coronas contain thick, almost-straight channels with extensions of up to one meter (P. O. Kochkin et al., 2014; Kostinskiy et al., 2018). Although these channels are surrounded by smaller streamers, there is no reason to believe that these short bifurcations play an essential role in the dynamics of the main channel. Interestingly, this is not the case for positive coronas (P. O. Kochkin, Nguyen, van Deursen, & Ebert, 2012; Kostinskiy et al., 2018), which may be yet another reason for the polarity asymmetry in leader propagation.

Our results explain the formation of brighter and warmer inhomogeneities ahead of a negative leader channel. This is the first stage in the streamer-to-leader transition in a stepped leader. The subsequent evolution of the space stem is still not understood: namely we do not know the mechanism that maintains the corona conductivity long enough to reach thousands of degrees. A full understanding of lightning progression and associated phenomena such as the emission of X-rays will only result from the successful investigation of this mechanism.

Acknowledgments

Information on how to access the code used to run the simulations as well as the output data analyzed in this study is available in the supporting information. This work was supported by the European Research Council (ERC) under the European Union H2020 programme/ERC grant agreement 681257. A. Malagón-Romero and A. Luque acknowledge financial support from the State Agency for Research of the Spanish MCIU through the "Center of Excellence Severo Ochoa" award for the Instituto de Astrofísica de Andalucía(SEV-2017-0709). We acknowledge Prof. U. Ebert for useful discussions about the contents of this paper.

References

- Alghamdi, A., Ahmadi, A., Ketcheson, D. I., Knepley, M. G., Mandli, K. T., & Dalcin, L. (2011). Petclaw: A scalable parallel nonlinear wave propagation solver for python. In *Proceedings of the 19th high performance computing symposia* (pp. 96–103). San Diego, CA, USA: Society for Computer Simulation International. Retrieved from <http://dl.acm.org/citation.cfm?id=2048577.2048590>
- Babich, L., & Bochkov, E. (2017). Numerical simulation of electric field enhancement at the contact of positive and negative streamers in relation to the problem of runaway electron generation in lightning and in long laboratory sparks. *J. Phys. D*, 50, 455202.

- doi: 10.1088/1361-6463/aa88fd
- Babich, L. P., Bochkov, E. I., Kutsyk, I. M., Neubert, T., & Chanrion, O. (2015). A model for electric field enhancement in lightning leader tips to levels allowing X-ray and γ ray emissions. *J. Geophys. Res. (Space Phys)*, 120, 5087. doi: 10.1002/2014JA020923
- Balay, S., Abhyankar, S., Adams, M. F., Brown, J., Brune, P., Buschelman, K., ... Zhang, H. (2016a). *PETSc users manual* (Tech. Rep. No. ANL-95/11 - Revision 3.7). Argonne National Laboratory. Retrieved from <http://www.mcs.anl.gov/petsc>
- Balay, S., Abhyankar, S., Adams, M. F., Brown, J., Brune, P., Buschelman, K., ... Zhang, H. (2016b). *PETSc Web page*. <http://www.mcs.anl.gov/petsc>. Retrieved from <http://www.mcs.anl.gov/petsc>
- Bazelyan, E., & Raizer, Y. (2010). *Lightning physics and lightning protection*. Bristol, UK: Institute of Physics Publishing.
- Biagi, C. J., Uman, M. A., Hill, J. D., & Jordan, D. M. (2014). Negative leader step mechanisms observed in altitude triggered lightning. *J. Geophys. Res. (Atmos.)*, 119, 8160. doi: 10.1002/2013JD020281
- Biagi, C. J., Uman, M. A., Hill, J. D., Jordan, D. M., Rakov, V. A., & Dwyer, J. (2010). Observations of stepping mechanisms in a rocket-and-wire triggered lightning flash. *J. Geophys. Res. (Atmos.)*, 115, D23215. doi: 10.1029/2010JD014616
- Briggs, M. S., Xiong, S., Connaughton, V., Tierney, D., Fitzpatrick, G., Foley, S., ... Hutchins, M. L. (2013). Terrestrial gamma-ray flashes in the Fermi era: Improved observations and analysis methods. *J. Geophys. Res. (Space Phys)*, 118, 3805. doi: 10.1002/jgra.50205
- Capitelli, M., M., F. C., F., G. B., & I., O. A. (2000). *Plasma Kinetics in Atmospheric Gases*. Berlin, Germany: Springer Verlag.
- Clawpack Development Team. (2017). *Clawpack software*. Retrieved from <http://www.clawpack.org> (Version 5.4.1) doi: 10.5281/zenodo.820730
- Cooray, V. (2003). Mechanism of electrical discharges. In V. Cooray (Ed.), *The lightning flash*. Institution of Engineering and Technology.
- da Silva, C. L., & Pasko, V. P. (2013). Dynamics of streamer-to-leader transition at reduced air densities and its implications for propagation of lightning leaders and gigantic jets. *J. Geophys. Res. (Atmos.)*, 118, 13. doi: 10.1002/2013JD020618
- Douglas-Hamilton, D. H., & Mani, S. A. (1974). Attachment instability in an externally ionized discharge. *J. Appl. Phys.*, 45, 4406. doi: 10.1063/1.1663065
- Dwyer, J. R., Rassoul, H. K., Al-Dayeh, M., Caraway, L., Chrest, A., Wright, B., ... Rambo, K. J. (2005). X-ray bursts associated with leader steps in cloud-to-ground lightning. *Geophys. Res. Lett.*, 32, L01803. doi: 10.1029/2004GL021782

- Dwyer, J. R., & Uman, M. A. (2014). The physics of lightning. *Phys. Rep.*, 534, 147. doi: 10.1016/j.physrep.2013.09.004
- Ebert, U., Nijdam, S., Li, C., Luque, A., Briels, T., & van Veldhuizen, E. (2010). Review of recent results on streamer discharges and discussion of their relevance for sprites and lightning. *J. Geophys. Res. (Space Phys)*, 115, A00E43. doi: 10.1029/2009JA014867
- Fishman, G. J., Bhat, P. N., Mallozzi, R., Horack, J. M., Koshut, T., Kouveliotou, C., ... Christian, H. J. (1994). Discovery of Intense Gamma-Ray Flashes of Atmospheric Origin. *Science*, 264, 1313. doi: 10.1126/science.264.5163.1313
- Flitti, A., & Pancheshnyi, S. (2009). Gas heating in fast pulsed discharges in N₂-O₂ mixtures. *European Physical Journal Applied Physics*, 45(2), 21001. doi: 10.1051/epjap/2009011
- Gallimberti, I. (1979). The mechanism of the long spark formation. *Journal de Physique*, 40, 193.
- Gamerota, W. R., Idone, V. P., Uman, M. A., Ngin, T., Pilkey, J. T., & Jordan, D. M. (2014). Dart-stepped-leader step formation in triggered lightning. *Geophys. Res. Lett.*, 41, 2204. doi: 10.1002/2014GL059627
- Gorin, B. N., Levitov, V. I., & Shkilev, A. V. (1976). Some principles of leader discharge of air gaps with a strong non-uniform field,. *IEE Conf. Publ.*, 143, 274–278.
- Hagelaar, G. J. M., & Pitchford, L. C. (2005). Solving the Boltzmann equation to obtain electron transport coefficients and rate coefficients for fluid models. *Plasma Sour. Sci. Technol.*, 14, 722. doi: 10.1088/0963-0252/14/4/011
- Hill, J. D., Uman, M. A., & Jordan, D. M. (2011). High-speed video observations of a lightning stepped leader. *J. Geophys. Res. (Atmos.)*, 116, D16117. doi: 10.1029/2011JD015818
- Ihaddadene, M. A., & Celestin, S. (2015). Increase of the electric field in head-on collisions between negative and positive streamers. *Geophys. Res. Lett.*, 42, 5644. doi: 10.1002/2015GL064623
- Kochkin, P., Lehtinen, N., van Deursen, A. . P. J., & Østgaard, N. (2016). Pilot system development in metre-scale laboratory discharge. *J. Phys. D*, 49, 425203. doi: 10.1088/0022-3727/49/42/425203
- Kochkin, P. O., Nguyen, C. V., van Deursen, A. P. J., & Ebert, U. (2012). Experimental study of hard x-rays emitted from metre-scale positive discharges in air. *J. Phys. D*, 45, 425202. doi: 10.1088/0022-3727/45/42/425202
- Kochkin, P. O., van Deursen, A. P. J., & Ebert, U. (2014). Experimental study of the spatio-temporal development of metre-scale negative discharge in air. *J. Phys. D*, 47(14), 145203. doi: 10.1088/0022-3727/47/14/145203
- Kochkin, P. O., van Deursen, A. P. J., & Ebert, U. (2015). Experimental study on hard x-rays

- emitted from metre-scale negative discharges in air. *J. Phys. D*, 48(2), 025205. doi: 10.1088/0022-3727/48/2/025205
- Köhn, C., Chanrion, O., & Neubert, T. (2017). Electron acceleration during streamer collisions in air. *Geophys. Res. Lett.*, 44, 2604. doi: 10.1002/2016GL072216
- Kossyi, I. A., Kostinsky, A. Y., Matveyev, A. A., & Silakov, V. P. (1992). Kinetic scheme of the non-equilibrium discharge in nitrogen-oxygen mixtures. *Plasma Sour. Sci. Technol.*, 1, 207. doi: 10.1088/0963-0252/1/3/011
- Kostinskiy, A. Y., Syssoev, V. S., Bogatov, N. A., Mareev, E. A., Andreev, M. G., Bulatov, M. U., ... Rakov, V. A. (2018). Abrupt elongation (stepping) of negative and positive leaders culminating in an intense corona streamer burst: Observations in long sparks and implications for lightning. *J. Geophys. Res. (Atmos.)*. Retrieved from <https://agupubs.onlinelibrary.wiley.com/doi/abs/10.1029/2017JD027997> doi: 10.1029/2017JD027997
- Landau, L., & Lifshitz, E. (1987). *Fluid mechanics* (Second ed.). Pergamon Press. Retrieved from <https://books.google.es/books?id=CeBbAwAAQBAJ>
- Les Renardières group. (1978). Negative discharges in long air gaps at les renardières. *Elektra*, 74, 67–216.
- LeVeque, R. (2002). *Finite volume methods for hyperbolic problems*. Cambridge University Press.
- Liu, N. (2010). Model of sprite luminous trail caused by increasing streamer current. *Geophys. Res. Lett.*, 37, L04102. doi: 10.1029/2009GL042214
- Liu, N., Kosar, B., Sadighi, S., Dwyer, J. R., & Rassoul, H. K. (2012). Formation of Streamer Discharges from an Isolated Ionization Column at Subbreakdown Conditions. *Phys. Rev. Lett.*, 109(2), 025002. doi: 10.1103/PhysRevLett.109.025002
- Luque, A. (2017). Radio Frequency Electromagnetic Radiation From Streamer Collisions. *J. Geophys. Res. (Atmos.)*, 122, 10. doi: 10.1002/2017JD027157
- Luque, A., & Ebert, U. (2010). Sprites in varying air density: Charge conservation, glowing negative trails and changing velocity. *Geophys. Res. Lett.*, 37, L06806. doi: 10.1029/2009GL041982
- Luque, A., & Ebert, U. (2014). Growing discharge trees with self-consistent charge transport: the collective dynamics of streamers. *New Journal of Physics*, 16(1), 013039. doi: 10.1088/1367-2630/16/1/013039
- Luque, A., Ebert, U., Montijn, C., & Hundsdoerfer, W. (2007). Photoionization in negative streamers: Fast computations and two propagation modes. *Appl. Phys. Lett.*, 90(8), 081501. doi: 10.1063/1.2435934
- Luque, A., González, M., & Gordillo-Vázquez, F. J. (2017). Streamer discharges as advancing imperfect conductors: inhomogeneities in long ionized channels. *Plasma Sour. Sci.*

- Technol.*, 26(12), 125006. doi: 10.1088/1361-6595/aa987a
- Luque, A., & Gordillo-Vázquez, F. J. (2011). Sprite beads originating from inhomogeneities in the mesospheric electron density. *Geophys. Res. Lett.*, 38, L04808. doi: 10.1029/2010GL046403
- Luque, A., Ratushnaya, V., & Ebert, U. (2008). Positive and negative streamers in ambient air: modelling evolution and velocities. *J. Phys. D*, 41(23), 234005. doi: 10.1088/0022-3727/41/23/234005
- Luque, A., Stenbaek-Nielsen, H. C., McHarg, M. G., & Haaland, R. K. (2016). Sprite beads and glows arising from the attachment instability in streamer channels. *J. Geophys. Res. (Space Phys)*, 121. doi: 10.1002/2015JA022234
- Malagón-Romero, A., & Luque, A. (2018). A domain-decomposition method to implement electrostatic free boundary conditions in the radial direction for electric discharges. *Comput. Phys. Commun.*, 225, 114. doi: 10.1016/j.cpc.2018.01.003
- Marisaldi, M., Argan, A., Trois, A., Giuliani, A., Tavani, M., Labanti, C., . . . Salotti, L. (2010). Gamma-Ray Localization of Terrestrial Gamma-Ray Flashes. *Phys. Rev. Lett.*, 105(12), 128501. doi: 10.1103/PhysRevLett.105.128501
- Nijdam, S., Takahashi, E., Markosyan, A. H., & Ebert, U. (2014). Investigation of positive streamers by double-pulse experiments, effects of repetition rate and gas mixture. *Plasma Sour. Sci. Technol.*, 23(2), 025008. doi: 10.1088/0963-0252/23/2/025008
- Orville, R. E. (1968). Spectrum of the lightning stepped leader. *J. Geophys. Res.*, 73, 6999. doi: 10.1029/JB073i022p06999
- Østgaard, N., Carlson, B. E., Nisi, R. S., Gjesteland, T., Grondahl, O., Skeltved, A., . . . Kochkin, P. (2016). Relativistic electrons from sparks in the laboratory. *J. Geophys. Res. (Atmos.)*, 121, 2939. doi: 10.1002/2015JD024394
- Phelps, C. T. (1974). Positive streamer system intensification and its possible role in lightning initiation. *Journal of Atmospheric and Terrestrial Physics*, 36, 103. doi: 10.1016/0021-9169(74)90070-1
- Popov, N. A. (2001). Investigation of the Mechanism for Rapid Heating of Nitrogen and Air in Gas Discharges. *Plasma Physics Reports*, 27, 886. doi: 10.1134/1.1409722
- Popov, N. A. (2003). Formation and development of a leader channel in air. *Plasma Physics Reports*, 29, 695. doi: 10.1134/1.1601648
- Rison, W., Krehbiel, P. R., Stock, M. G., Edens, H. E., Shao, X.-M., Thomas, R. J., . . . Zhang, Y. (2016). Observations of narrow bipolar events reveal how lightning is initiated in thunderstorms. *Nature Communications*, 7, 10721. doi: 10.1038/ncomms10721
- Schonland, B. F. J., Malan, D. J., & Collens, H. (1935). Progressive Lightning. II. *Proc. R. Soc. London, Ser. A*, 152, 595. doi: 10.1098/rspa.1935.0210

- Shi, F., Liu, N., & Dwyer, J. R. (2017). Three-Dimensional Modeling of Two Interacting Streamers. *J. Geophys. Res. (Atmos.)*, 122, 10. doi: 10.1002/2017JD026935
- Sigmond, R. S. (1984). The residual streamer channel: Return strokes and secondary streamers. *J. Appl. Phys.*, 56, 1355. doi: 10.1063/1.334126
- Smith, D. M., Lopez, L. I., Lin, R. P., & Barrington-Leigh, C. P. (2005). Terrestrial Gamma-Ray Flashes Observed up to 20 MeV. *Science*, 307, 1085. doi: 10.1126/science.1107466
- Teunissen, J., & Ebert, U. (2017). Simulating streamer discharges in 3D with the parallel adaptive Afivo framework. *J. Phys. D*, 50, 474001. doi: 10.1088/1361-6463/aa8faf
- Thomas, R. J., Krehbiel, P. R., Rison, W., Hamlin, T., Harlin, J., & Shown, D. (2001). Observations of VHF source powers radiated by lightning. *Geophys. Res. Lett.*, 28, 143. doi: 10.1029/2000GL011464
- Wormeester, G., Pancheshnyi, S., Luque, A., Nijdam, S., & Ebert, U. (2010). Probing photoionization: simulations of positive streamers in varying N₂ : O₂-mixtures. *J. Phys. D*, 43, 505201. doi: 10.1088/0022-3727/43/50/505201
- Zhelezniak, M. B., Mnatsakanian, A. K., & Sizykh, S. V. (1982). Photoionization of nitrogen and oxygen mixtures by radiation from a gas discharge. *High Temperature Science*, 20, 423.

Supporting information for
**Spontaneous emergence of space stems ahead of negative
leaders in lightning and long sparks**

A. Malagón-Romero,¹ A. Luque¹

Corresponding author: A. Malagón-Romero, IAA-CSIC, P.O. Box 3004, 18080 Granada, Spain.
(amaro@iaa.es)

¹IAA-CSIC, P.O. Box 3004, 18080 Granada,
Spain.

arXiv:1909.04424v1 [physics.ao-ph] 10 Sep 2019

Contents of this file

1. Text S1 to S3

2. Figures S1 to S3

3. Table S1

Introduction

This supporting information provides details of the chemistry accounting for the light emissions (Text S1), a description of a simplified model for a leader corona (Text S2) that supplements the main scientific conclusions of the paper and a summary about the numerical implementation of the methods used in this work (Text S3). S2 contains three subsections: a) In S2a we describe the model itself, b) in S2b we set up the model to account for a single corona discharge while in c) S2c, the settings pursue multiple discharges. Table S1 provides the parameter values employed in our simulations. Figures S1 and S2 show the main output of the model for a single and multiple corona discharges respectively. The data supporting the findings of this study are available at:

<https://cloud.iaa.csic.es/public.php?service=files&t=4a1b59a05ffed44c475518a39300abac>

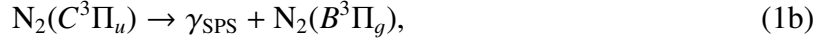
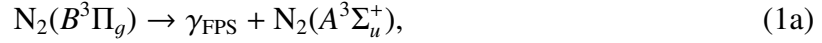
The code to obtain the output data that we have analyzed here is available at:

https://gitlab.com/amaro/space_stem.git

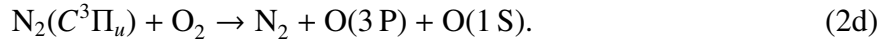
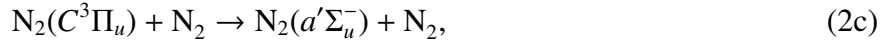
Text S1. Light Emissions

Our discharge develops in a high pressure regime (atmospheric pressure), therefore the dynamics of the charged species is heavily dominated by collisions. A fraction of these collisions excites electronic states such as $N_2(B^3\Pi_g)$ and $N_2(C^3\Pi_u)$. These electronically excited states

undergo radiative deactivation:



and produce emissions known as First Positive System (FPS) and Second Positive System (SPS) respectively. These species can also be collisionally quenched:



In our code we used electron impact excitation rates for reactions (1) obtained from BOLSIG+ Hagelaar and Pitchford (2005) using the cross-section database Phelps (n.d.). The reaction rates for the collisional quenching reactions (2) have been obtained from Capitelli, M., F., and I. (2000).

Text S2. Two-Sphere Model for a Leader Corona

In the main text we described in detail the initial 100 ns of the streamer-to-leader transition. This time is sufficient to establish the space stem but it is clearly too short to reach the characteristic temperatures inside a leader. Unfortunately, for the reasons explained in the main text, currently microscopical models cannot be extended to long times. However we may obtain a glimpse of the most important physics at these longer timescales.

We present here a streamlined and heavily simplified model of the corona ahead of a leader. Although it is clearly insufficient to produce accurate predictions, it illustrates the physics of the

streamer-to-leader transition shows two things: (1) that for the streamer-to-leader transition to occur there must be a mechanism that either creates new streamers or increases the conductivity of existing channels by means of consecutive ionization waves and (2) that a small difference in initial electron density in the stem leads to large differences in the heating rate of this segment compared to the rest of the corona.

Text S2a. Model Description

The model's geometry is sketched in figure S1. The leader tip is mimicked by a conducting sphere of radius a at a potential V_L , whereas the electrical charge in the corona is distributed within another sphere with radius b . The centers of the two spheres are separated by a length L . In order to simplify our calculations we assume that the corona sphere has a uniform potential V_C arising from a total corona charge Q_C . The electrostatic system of two conducting spheres with potentials V_L , V_C and charges Q_L and Q_C is defined by a capacitance matrix C such that

$$\begin{pmatrix} Q_L \\ Q_C \end{pmatrix} = \begin{pmatrix} C_{LL} & C_{LC} \\ C_{CL} & C_{CC} \end{pmatrix} \begin{pmatrix} V_L \\ V_C \end{pmatrix}, \quad (3)$$

where the elements of C can be calculated by repeated application of the method of images.

From (3) we obtain

$$V_C = -\frac{C_{CL}}{C_{CC}} V_L + \frac{Q_C}{C_{CC}}. \quad (4)$$

The two spheres are connected by streamer channels, which this model represents as linear electrical resistors. Of these, N are identical, unperturbed resistors of length L (we neglect differences in these distances) whereas one perturbed channel contains the space stem and is thus divided into three serially connected resistors: the space stem, of length ℓ is surrounded by two channels of length $(L - \ell)/2$.

The current inside each resistor is generated by the drift of current carriers, each with mobility μ_s , where $s = 1, \dots$ indexes the species (this includes electrons and positive and negative ions). The underlying charge carrier densities and mobilities in the streamers are respectively $n_{0,s}$ in the unperturbed, long channels, $n_{\text{stem},s}$ in the stem and $n_{1,s}$ in the two channel segments surrounding the stem. These densities are uniform within the channels, all of them of cylindrical shape and with a radius r .

Assuming now that the electric field that drives the charge carriers inside each channel can be approximated by its average, we obtain the current in the unperturbed channels as

$$I_0 = \frac{\pi r^2 e (V_L - V_C)}{L} \sum_s \mu_s n_{0,s} = \frac{V_L - V_C}{R_0}, \quad (5)$$

where the resistance R_0 is defined as

$$R_0 = \frac{L}{\pi r^2 e} \left(\sum_s \mu_s n_{0,s} \right)^{-1}. \quad (6)$$

Defining similarly the resistance of the stem as

$$R_{\text{stem}} = \frac{\ell}{\pi r^2 e} \left(\sum_s \mu_s n_{\text{stem},s} \right)^{-1}, \quad (7)$$

and that of the two channel surrounding the stem as

$$R_1 = \frac{(L - \ell)}{2\pi r^2 e} \left(\sum_s \mu_s n_{1,s} \right)^{-1}, \quad (8)$$

yields for the current in the perturbed channel

$$I_1 = \frac{V_L - V_C}{R_{\text{stem}} + 2R_1}. \quad (9)$$

The charge accumulation in the corona then follows

$$\frac{dQ_C}{dt} = NI_0 + I_1. \quad (10)$$

The species densities evolve according to the chemical system described in the main text subjected to electric fields averaged over the extension of each path, which can be calculated from Ohm's law as $\bar{E}_c = R_c I_c / l_c$, where c indicates the kind of channel (unperturbed, stem or stem-neighbors) and l_c is the channel's length. Furthermore, each channel dissipates energy at a rate $R_c I_c^2$ and therefore its temperature increases at a rate

$$\frac{dT}{dt} = \frac{\eta R_c I_c^2}{\pi r^2 l_c n_{\text{air}} c_V}, \quad (11)$$

where n_{air} is the number density of air at standard temperature and pressure and c_V is the specific heat capacity of air, which we take as $c_V = (5/2)k$, k being Boltzmann's constant. As in the main text, η stands for the fraction of energy deposited into thermalized degrees of freedom; we take here too $\eta = 1/2$.

Note that as the stem heats up some processes that are not included in our chemical model, such as vibrational-translational relaxation, play an increasingly significant role. Therefore high temperatures in this simplified model cannot be considered as quantitative predictions.

The parameters used in the following simulations are listed in table S1. As initial conditions we set an electron density $n_e = 10^{19} \text{ m}^{-3}$, balanced by N_2^+ and O_2^+ in a ratio matching the air fractions of molecular nitrogen and oxygen. In the "stem" resistor this initial density is reduced by a factor 0.75. Once this different initial condition is set, all resistor follow the same evolution equations. Note that our input values have not been fine-tuned to obtain the results described below.

Text S2b. Single Corona Discharge

As a first step, let us check that results from this simplified model are broadly consistent with the fluid model described in the main text. Figure S2 shows the evolution of the most relevant

variables of the model. The main result is that, as we noticed in the main text, the electron density is depleted with a timescale of around 100 ns. Hence the temperature in any of the channels does not increase further than a few Kelvin. However, the small perturbation in electron density introduced in the “stem” channel is sufficient to excite the attachment instability described in the paper and thus drives this component to higher electric fields and more dissipation. The increase in temperature is thus significantly higher in this segment but still far below that needed to transition to a leader.

Note however that the potential drop between the leader and the corona has barely bulged and there is still a high potential in the leader that is available to initiate new discharges.

Text S2c. Multiple Discharges

We hypothesize that the large electrostatic potential remaining at the leader tip after the electron density has been depleted generates subsequent ionization waves that prevent the conductivity region ahead of the leader tip to disappear completely. To substantiate this hypothesis we provide here an example of how the physics of the streamer-to-leader transition may work on long timescales after the space stem has formed.

Assume then that due to its high potential, the leader tip launches successive streamer-like ionization waves that propagate along or close to previous existing channels. A similar process was observed by Nijdam, Takahashi, Markosyan, and Ebert (2014). As an example, let us assume that these waves are launched every 100 ns and that their effect is to increase the channel ionization by a factor 10. Given their fast timescales, these ionization waves can be implemented in our model by instantaneous increases of the electron and ion densities.

The result is plotted in figure S3, where we show the evolution of the system after 10 ionization waves. The gas heating in this case is stronger, with the stem reaching a temperature close to 800 K compared to only about 400 K for the rest of the corona channels.

Text S3. Numerical Implementation

In the form used in this work, the compressible Euler equations are hyperbolic equations with additional source terms. Finite Volume Methods are suitable to solve these equations once the source terms are properly treated. To solve these equations we have used CLAWPACK/PETCLAW (Alghamdi et al., 2011; Clawpack Development Team, 2017; LeVeque, 2002). PETCLAW is built upon PETSc (Balay et al., 2016a, 2016b) and allows us to split the simulation domain into different subdomains (problems) that can be solved in parallel. The Poisson’s equation is solved using the Improved Stabilized version of BiConjugate Gradient solver from the PETSc numerical library. The space resolution was $25\text{ }\mu\text{m}$ and we used an adaptive time-step constrained by a Courant-Friedrichs-Levy number of 0.005 and by the shortest chemical time-scale $\tau_s = n_s(dn_s/dt)^{-1}$ among all species s .

References

- Alghamdi, A., Ahmadi, A., Ketcheson, D. I., Knepley, M. G., Mandli, K. T., & Dalcin, L. (2011). Petclaw: A scalable parallel nonlinear wave propagation solver for python. In *Proceedings of the 19th high performance computing symposia* (pp. 96–103). San Diego, CA, USA: Society for Computer Simulation International. Retrieved from <http://dl.acm.org/citation.cfm?id=2048577.2048590>
- Balay, S., Abhyankar, S., Adams, M. F., Brown, J., Brune, P., Buschelman, K., ... Zhang, H. (2016a). *PETSc users manual* (Tech. Rep. No. ANL-95/11 - Revision 3.7). Argonne

143 National Laboratory. Retrieved from <http://www.mcs.anl.gov/petsc>

144 Balay, S., Abhyankar, S., Adams, M. F., Brown, J., Brune, P., Buschelman, K., ... Zhang,

145 H. (2016b). *PETSc Web page*. <http://www.mcs.anl.gov/petsc>. Retrieved from

146 <http://www.mcs.anl.gov/petsc>

147 Capitelli, M., M., F. C., F., G. B., & I., O. A. (2000). *Plasma Kinetics in Atmospheric Gases*.

148 Berlin, Germany: Springer Verlag.

149 Clawpack Development Team. (2017). *Clawpack software*. Retrieved from <http://www>

150 [.clawpack.org](http://www.clawpack.org) (Version 5.4.1) doi: 10.5281/zenodo.820730

151 Hagelaar, G. J. M., & Pitchford, L. C. (2005). Solving the Boltzmann equation to obtain

152 electron transport coefficients and rate coefficients for fluid models. *Plasma Sour. Sci.*

153 *Technol.*, 14, 722. doi: 10.1088/0963-0252/14/4/011

154 LeVeque, R. (2002). *Finite volume methods for hyperbolic problems*. Cambridge University

155 Press.

156 Nijdam, S., Takahashi, E., Markosyan, A. H., & Ebert, U. (2014). Investigation of positive

157 streamers by double-pulse experiments, effects of repetition rate and gas mixture. *Plasma*

158 *Sour. Sci. Technol.*, 23(2), 025008. doi: 10.1088/0963-0252/23/2/025008

159 Phelps, A. V. (n.d.). *Compilation of cross-sections*. Retrieved from <ftp://jila.colorado>

160 [.edu/collision_data/](ftp://jila.colorado.edu/collision_data/)

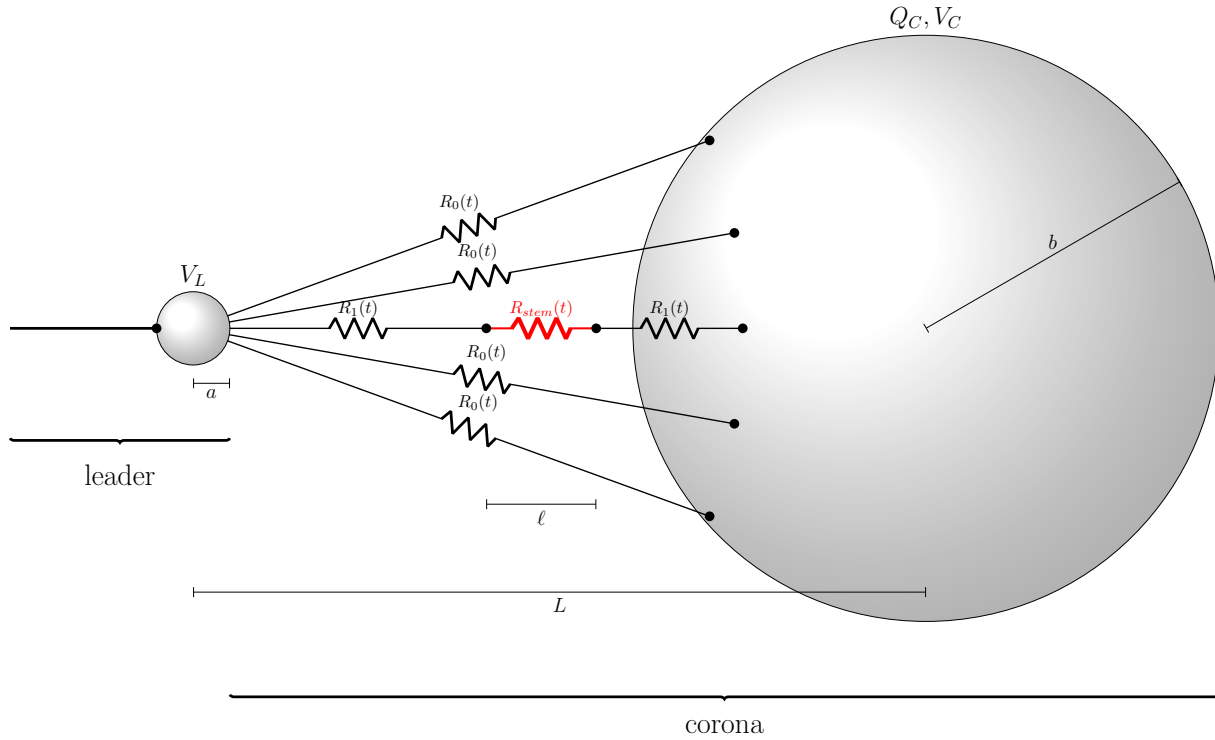


Figure S1. Sketch of the model. Two conducting spheres, representing respectively the leader tip and the corona space charge are connected by channels representing the streamer discharges. Most of these channels are uniform and modeled as single resistors. One of the channels is perturbed to contain a space stem, represented by a different resistor (shown in red).

Parameter	Value
L	1 m
a	1 cm
b	25 cm
r	0.5 mm
V_L	1 MV
N	50

Table S1. Parameter values employed in our simulations.

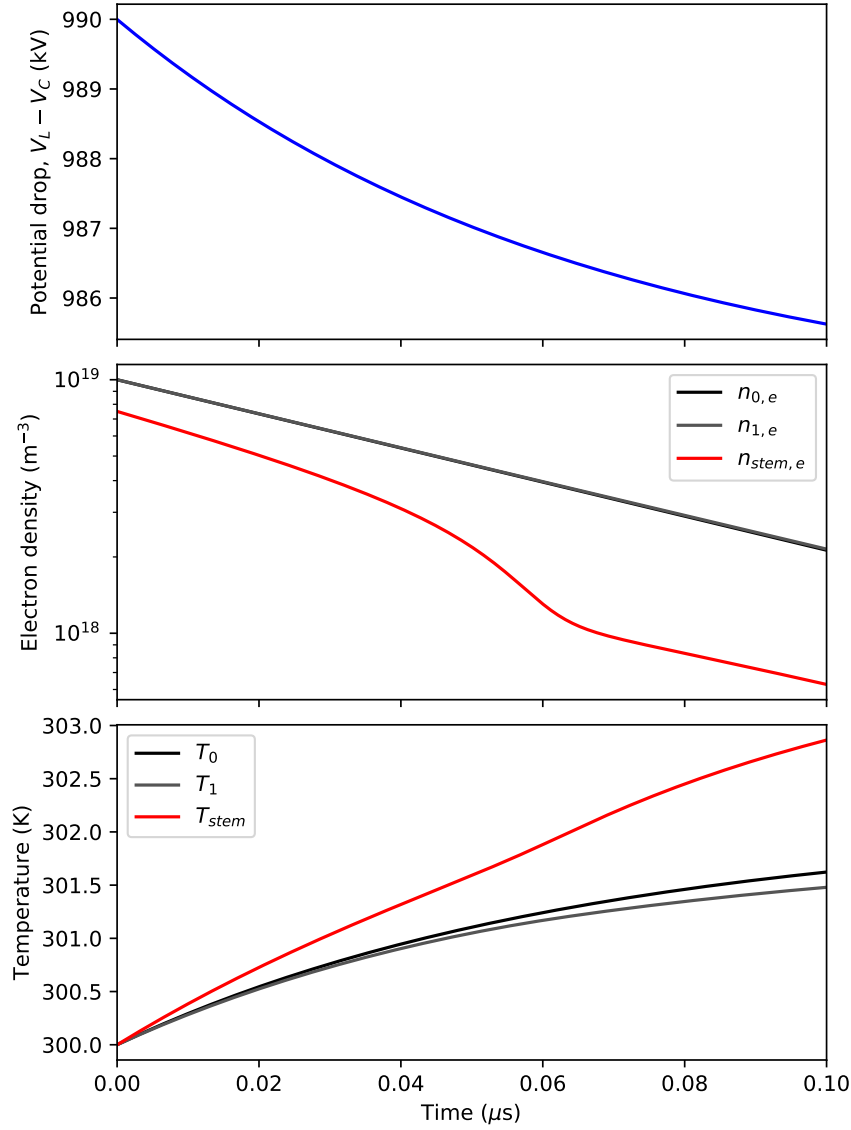


Figure S2. Simulation of a single corona discharge in the two-sphere model. Here we show 100 ns of simulation. The top panel shows a small decrease in the potential drop; the central panel shows that the electron density decays quickly, faster in the space stem than in the other channels. Finally, the lower panel plots a small increase of gas temperature, which is nevertheless much more significant in the stem.

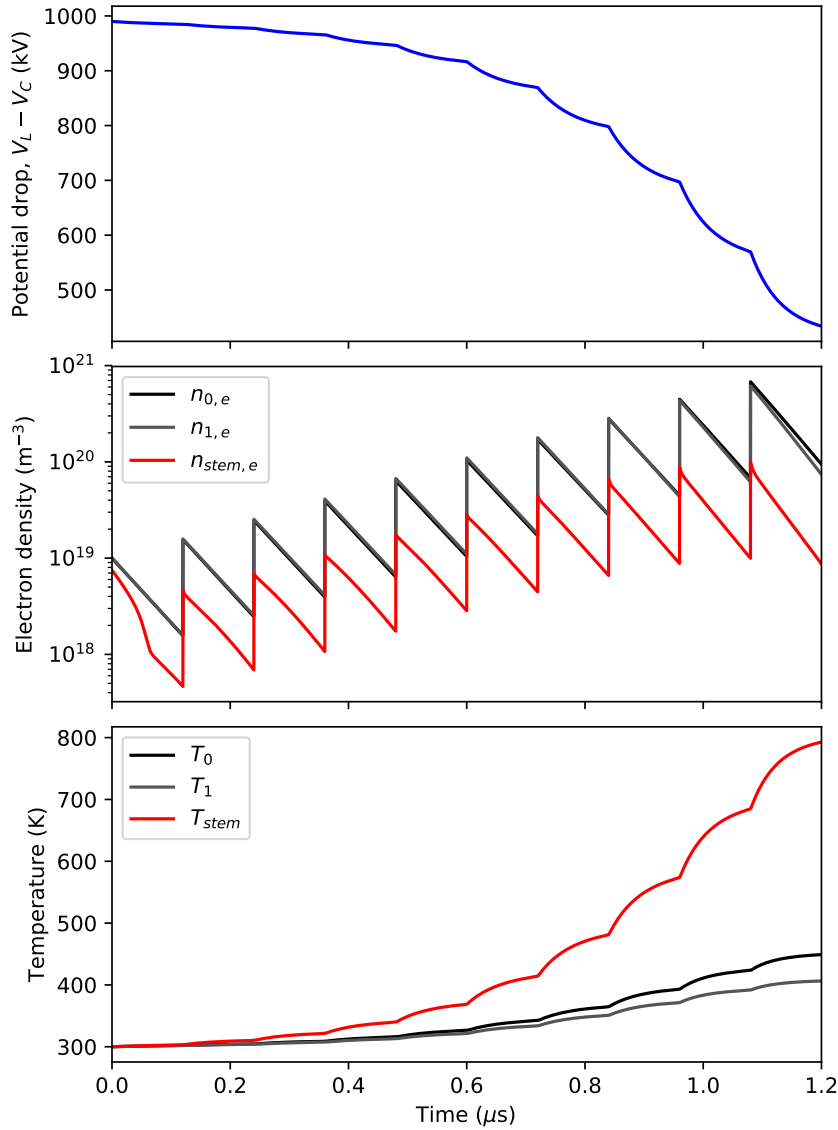


Figure S3. Corona discharge followed by multiple ionization waves that sustain a high ionization in the streamer channels. In this case the electrostatic potential drop (top panel) decays significantly, whereas the electron density (middle panel) increases slowly. The temperature of the channels (lower panel) increases up to around 800 K for the stem and only to around 400 K for the rest of the channels.